Investigation of the Three-Dimensional Turbulent Flow Fields of the Gas Swirl Burner with a Cone Type Baffle Plate (I)

Jang-kweon Kim*

Department of Marine Engineering, Kunsan National University, Chonbuk 573-702, Korea

This paper presents vector fields, three dimensional mean velocities, turbulent intensities, turbulent kinetic energy and Reynolds shear stresses measured in the X-Y plane of the gas swirl burner with a cone type baffle plate by using an X-type hot-wire probe. This experiment is carried out at the flow rates of 350 and 450 ℓ/min which are equivalent to the combustion air flow rate necessary to release 15,000 kcal/hr in a gas furnace. The results show that the maximum axial mean velocity component exists around the narrow slits situated radially on the edge of a burner. Therefore, there is some entrainment of ambient air in the outer region of a burner. The maximum values of turbulent intensities occur around the narrow slits and in front of a burner up to X/R=1.5. Moreover, the turbulent intensity components show a relatively large value in the inner region due to the flow diffusion and mixing processes between the inclined baffle plate and the swirl vane. Consequently, the combustion reaction is expected to occur actively near these regions.

Key Words : Gas Swirl Burner, Hot-Wire Anemometer, Streamline, Subsonic Wind Tunnel, Turbulent Flow Fields, Vector, X-Probe

Nomenclature

D_I	: Inner diameter of a swirl vane [m]
D_o	: Outer diameter of a swirl burner [m]
k_1, k_2	: Mean yaw factor of sensor 1 and 2 [−]
KE	: Turbulent kinetic energy [m^2/s^2]
Q	: Air flow rate [m^3/min]
R	: Radius of a swirl burner [m]
S_n	: Swirl number [−]
U, V, W	: Mean velocity component in the X, Y and Z direction respectively [m/s]
u, v, w	: Root mean square of turbulent fluctuation velocity in the X, Y and Z direction respectively [m/s]
U_o	: Upstream mean velocity of a swirl burner ($=Q/\pi R^2$) [m/s]
U_1, U_2	: Response flow velocity obtained from sensor 1 and 2 respectively in the hot-wire coordinate system [m/s]
U_{1cal}, U_{2cal}	: Calibration flow velocity on the flow velocities U_1 and U_2 in the hot-wire anemometer system [m/s]
uv, uw	: Reynolds shear stress components [m^2/s^2]
X, Y, Z	: Distance and direction of cartesian coordinate system
α	: Swirl vane angle [°]
α_1, α_2	: Angles between each sensor (1, 2) and probe coordinate system [°]

* **E-mail** : flowkim@kunsan.ac.kr
TEL : +82-63-469-1848 ; **FAX** : +82-63-469-1841
Department of Marine Engineering, Kunsan National University, 1044-2, So-ryong Dong, Kunsan, Chonbuk 573-702, Korea. (Manuscript **Recieved** September 2, 2000; **Revised** March 8, 2001)

1. Introduction

Recently, the supplies of cars, airplanes, ships, plants and apartments etc. are continuously increasing due to the rapid improvement of the standard of living. Therefore, the energy consumption is also increasing. The excess energy consumption causes air pollution and global warming. Therefore, the efficiency of combustors

and various engines need to be improved to save energy and protect the environment.

The combustion characteristics of combustors using a gas burner depend on various parameters such as the composition of fuel gas, the diffusion of the ejected gas, and the mixing between air and fuel gas etc. Above all, the mixing rate between air and fuel gas is thought to become more important parameter than the others in combustion state. In addition, there are many parameters of the angle, the inner and outer radius of a swirl vane, and the shape of flame holder as to the optimum parameter for burner design. On the other hand, the efforts for improving combustion property by changing the burner geometry are actively progressing at home and abroad.

Aoki et al. (1988, 1989) experimentally clarified the location, size and shape of recirculation, the eye of vortex and sub-recirculation zones for the swirling numbers, and the maximum reverse flow rate of recirculation zone on the circular duct flow superposed with swirling flow. In order to analyze these results, they used flow visualization by spark tracing method for clearing flow patterns, five-hole pitot-tube, and LDA (Laser Doppler Anemometer) system for measuring three time-mean velocities and turbulent characteristics respectively when the swirling numbers change from zero to 1.35 by an axial flow type swirler.

Hirai et al. (1988) experimentally investigated the combustion characteristics capable of producing high combustion intensity and low environmental pollution to reduce NO_x emission from the burning of fine fuel spray formed by the twin-fluid atomizer that is generally utilized for an industrial boiler or furnace etc. They clarified that NO_x emission was affected by combustion states, burnt gas temperature and O_2 concentrations. Moreover, they also proved that NO_x emission attained to maximum values at the air excess ratio of $1.1 \sim 1.2$ for each combustion condition, but it was prominently reduced with increasing or decreasing in air excess ratio.

Ikeda et al. (1995) measured a flow velocity and gas species in combustion and non-combustion in an oil furnace by using LDA system. They showed that the reversing flow regions for both cases were located at the same place and their volumes were almost equal.

Kurihara et al. (1994, 1995) measured a droplet velocity in spray fields formed near the burner throat in the cold condition of an industrial oil burner which is a kind of gun-type burner, whose flame is stabilized by a baffle plate, by using PDA (Phase Doppler Anemometer) system to elucidate the interaction between turbulent air flow and spray. They showed that the behavior of droplets in the spray could be classified into three patterns by droplet diameters. The particles with a diameter smaller than 30 μm show a fluid motion and those with a diameter larger than 50 μm penetrate a turbulent airflow. On the other hand, the spray with droplets larger than 70 μm in diameter forms the hollow cone distribution that induces a shear flow along the spray. Then, the shear generates turbulence and the small droplets are drawn inside a hollow cone.

Kihm et al. (1990) investigated the flow characteristics of turbulent swirling flows with changing a hub diameter and a vane angle of swirler for a gas turbine by using LDA system. They observed that the peak tangential velocities were found at the exit of the swirler of 40°. These findings agreed to the result of direct force measurements of thrust and torque. In other words, they were found to be higher for the swirler of 40° than for the swirlers of 20° and 60°. The size and the strength of a recirculation zone were found to be highest at the swirler of 40°.

Kim et al. (1997, 1998) and Yoon (1999) introduced the experimental and numerical method to compare characteristics of flow fields with those of combustion fields according to the shape of flame holder with a vertical and an inclined baffle plate in a gun type oil and gas burner. They also verified that the flame holder with an inclined baffle plate formed more stable flame structure than that with a vertical baffle plate in the inner downstream region, and what is more, the hot temperature region attained in the downstream region of the swirl vane and the narrow slits situated radially on the edge of a

burner respectively.

In the present study, mean velocity, turbulent intensity, turbulent kinetic energy and Reynolds shear stress were measured and analyzed in the X-Y plane of three-dimensional turbulent flow fields formed from the gas swirl burner with a cone type baffle plate without flame and combustion chamber by using hot-wire anemometer system. These measurements were achieved at the combustion air flow rates of 350 and 450ℓ/min respectively. Here, the results of flow rate 450ℓ/min were only displayed because the non-dimensional characteristics between two results had a similar shape. (Kim et al., 2001)

The objective of this study is to grasp both the flow characteristics and the questions on the gas swirl burner with a cone type baffle plate. Afterwards, these design materials are due to use for the development of a new model after maintaining the optimum design data obtained from a conventional model. (Kim, 2001)

2. Structure of a Gas Swirl Burner

Figure 1 shows the detail structure of a gas swirl burner used in this study. This burner is due to apply in a gas furnace with heat release 15,000 kcal/hr.

The gas swirl burner used in the present study is characterized by the burner shape with the cone type baffle plate which is inclined about 45° to the front side of a circular tube. This cone type baffle plate is composed of eight swirl vanes located in the inclined baffle plate and eight narrow slits situated radially on the edge of the swirl burner that is just located above a swirl vane.

Generally, in the case of a swirler, it has been suggested that the swirl number is only dependent on the swirler geometry. Beer et al. (1972) first introduced this geometric swirl number as follows:

$$S_n=\frac{2}{3}\left[\frac{1-(D_i/D_o)^3}{1-(D_i/D_o)^2}\right]\tan\alpha \qquad (1)$$

Here, if we use this swirl number defined as Eq. (1), this swirl burner can be represented as the swirl number $S_n=0.34$, where the parameters used in this study are as follows: inner diameter of a swirl vane $D_i=25$ mm, outer diameter of a swirl vane $D_o=57.8$ mm, and swirl vane angle $\alpha=24°$.

Consequently, it can be thought that this gas swirl burner guides both circulation flow and swirl flow at the same time by eight swirl vanes located in the inclined plane and eight narrow slits situated radially on the edge of a swirl burner. However, because this burner has a comparatively small swirl number and the mean velocity at the narrow slit is larger than that at swirl vane, this burner can be considered to adopt

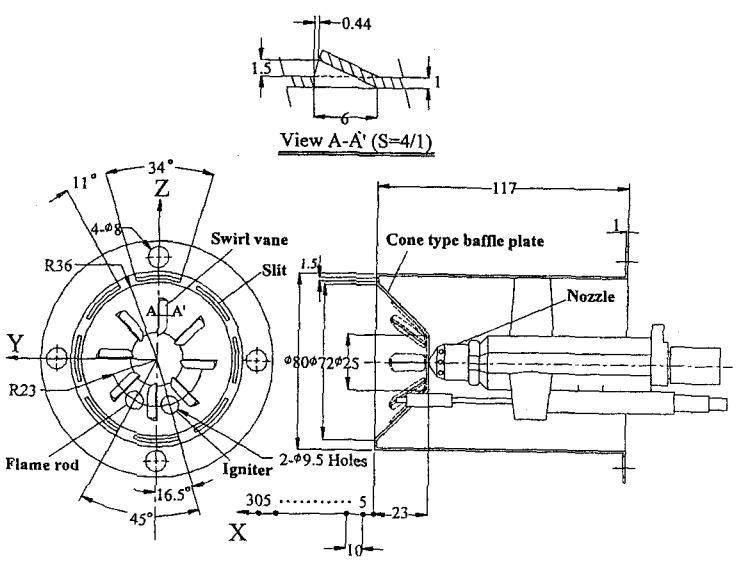

Fig. 1 Configuration of a gas swirl burner

the shape that generates the intense mixing between fuel gas and oxygen through strong turbulent intensity formed by large transverse slope of axial mean velocity at narrow slits rather than at swirl vanes.

3. Experimental Apparatus

Figure 2 shows the experimental apparatus diagram for measuring three-dimensional turbulent flow velocities by using hot-wire anemometer system from the swirl burner installed in the exit of test section of a subsonic wind tunnel.

This subsonic wind tunnel used in this study is composed of a centrifugal fan and a direct current type motor with a capacity of 3.75 kW (220 V, 3 Phase), a diffuser, a tranquilization, a contraction and a test section. Moreover, this subsonic wind tunnel shows the performance of maximum velocity 35 m/s in the test section having a size of 220 mm(width) x 220 mm(height) x 410 mm(length) and turbulent intensity under about 0.02 % at mean flow velocity 15 m/s.

Three-dimensional hot-wire anemometer system (Dantec 90N10 Streamline) used for measuring turbulent flow fields in the state of non-combustion is composed of three constant temperature hot-wire anemometers, a calibrator capable of doing velocity and directional calibration at the same time (Dantec 90H01 & 90H02), three-dimensional automatic traversing system (Dantec 41T50 & 41T75) and a personal computer (PC). Moreover, this hot-wire anemometer system is controlled through RS-232C interface by a PC, and the calibrator is connected by an air compressor capable of operating up to the extent of effective pressure of 10 kg/cm^2.

4. Experimental Method

4.1 Velocity calculation method by using an X-probe (Bruun, 1996; Dantec, 2000)

The measurement of three-dimensional velocity accomplished in this study by using an X-probe (Dantec, 55R51) from hot-wire anemometer system and PC is carried out as follows: if we assume that the velocities U_1 and U_2 are satisfied with sensor 1 and 2 respectively in the wire coordinate system of an X-probe, and moreover, the calibration velocities U_{1cal} and U_{2cal} correspond to the wire coordinate system, the equations for calculating the velocity components including the calibration velocities and the yaw-factors k_1 and k_2 for the wires are given as Eq. (2).

$$\begin{aligned} U_{1cal}^2 \times (1+k_1^2) \times \cos^2(90^\circ - \alpha_1) &= k_1^2 \times U_1^2 + U_2^2 \\ U_{2cal}^2 \times (1+k_2^2) \times \cos^2(90^\circ - \alpha_2) &= U_1^2 + k_2^2 \times U_2^2 \end{aligned} \quad (2)$$

where α_1 and α_2 are angles formed between each sensor and probe coordinate system, and they are composed of 45° respectively. Here, if we assume

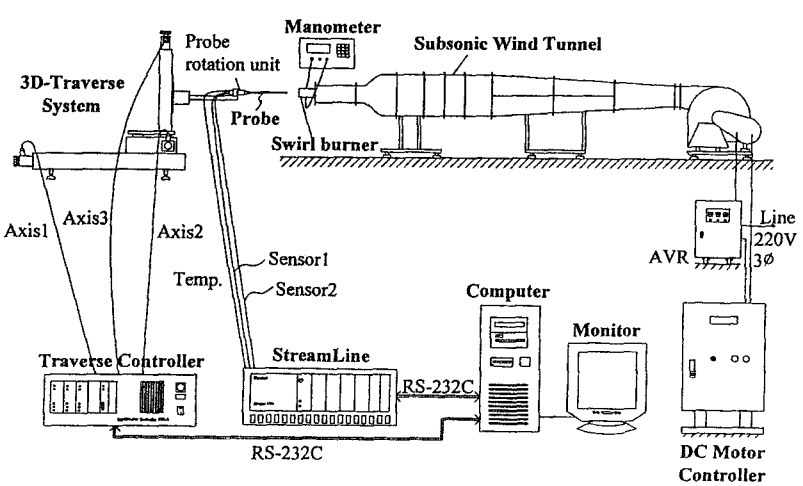

Fig. 2 Schematic diagram of experimental apparatus including hot-wire anemometer system

that the velocities U and V are satisfied with the probe coordinate system, the relationship between the velocities U_1 and U_2 of wire coordinate system and the velocities U and V of probe coordinate system can be defined as Eq. (3).

$$U = U_1 \times \cos\alpha_1 + U_2 \times \cos\alpha_2 \qquad (3)$$
$$V = U_1 \times \sin\alpha_1 - U_2 \times \sin\alpha_2$$

Therefore, the velocities U and V can be easily calculated if we insert them into Eq. (3) after solving Eq. (2) with respect to the velocities U_1 and U_2.

In this study, the calibration procedure with respect to the flow velocity and direction of an X-probe respectively was carried out through a calibrator connected with hot-wire anemometer system in order to acquire the calibration velocities and the yaw factors satisfied with Eq. (2) and Eq. (3). The velocity calibration was carried out by changing the velocity from zero to 20 m/s. Here, in view of the results achieved in the curve fit analysis of velocity calibration procedure by using the fifth order polynomial, we obtained the accuracy of velocity below about 0.4 % in this study. Moreover, the directional calibration with respect to X-probe was carried out by changing the yaw angle from $-40°$ to $+40°$ at 10-degree intervals with a constant flow velocity of 10 m/s. In consequence of the directional calibration procedure, the mean yaw factors were obtained as $k_1^2=0.064$ and $k_2^2=0.074$ respectively. On the other hand, the measurements of velocities U and W satisfied with the X-Y plane were carried out by counterclockwise rotating the X-probe through 90° around the axis of the probe installed for measuring the velocities U and V in the X-Y plane. The software of "Streamware" installed in PC automatically treats these all procedures.

4.2 Velocity measurement method within flow fields

The exit velocities of a swirl burner used in this study were respectively controlled under the static pressures of 98 Pa and 164 Pa collected from four pressure taps attached on the surface of the circular tube type swirl burner connected with the test section of a subsonic wind tunnel. Here, these static pressures respectively correspond to the flow rates of 350ℓ/min and 450ℓ/min which are utilized for actual combustion air flow rate. Moreover, these static pressures can be acquired when the auxiliary fan supplies the respective flow rate after connecting the swirl burner with a blow type fan tester. Here, the operation of a subsonic wind tunnel is continuously controlled until the static pressure on the surface of a swirl burner reaches a constant pressure established after warming up a centrifugal fan and motor satisfactorily. Afterwards, the normal velocity measurements were carried out by sampling enough many data from the turbulent flow fields formed at the respective measuring position in the X-Y plane after the velocity oscillation obtained from subsonic wind tunnel mostly disappears. The sampling frequency and the number of sampling of analog/digital converter used in this study are controlled with 10 kHz and 102,400 per channel respectively. Moreover, the frequency of low-pass filter of a signal conditioner was set up with 30 kHz per channel.

On the other hand, in order to measure the turbulent flow fields after fixing a desired measuring position, the following procedures were adopted for the present study. In other words, the method for installing X-probe in three-dimensional automatic traversing system was done with preserving the same direction and position as the geometry necessary for installing X-probe in a calibrator. Moreover, the main process for velocity measurements was accomplished after maintaining the precise origin between swirl burner and flow fields in the X-Y plane. Here, the setting up of the precise origin is carried out by checking mean velocity data acquired from hot-wire anemometer system with automatically traversing X-probe by 1 mm with respect to the horizontal and vertical direction respectively in front of a swirl burner as a reference of the geometric origin.

The gas swirl burner adopted in this study was used after eliminating flame rod and igniter installed in a cone type baffle plate and blocking their holes with a glue vinyl tape as shown in Fig. 1. The measuring position for moving X-probe in

the X-Y plane to X-direction was selected from 5 mm for protecting a sensor in front of a swirl burner to 305 mm at 10 mm intervals per position at the condition of respective flow rate because the shape of a swirl burner forms an axis of symmetry. On the other hand, the measuring position with respect to Y-direction was selected from −70 mm to 70 mm at 5 mm intervals per position around the origin of horizontal direction. Here, because the magnitude of velocity ejected from the eight narrow slits situated radially on the edge of a burner is the largest, the velocity measurements near these narrow slits were carried out with traversing X-probe by 1 mm to measure a detailed flow velocity. The room temperature was controlled within about 19±0.5 ℃ for reducing the error of velocity due to the change of temperature at the smallest possible value. In addition, the automatic voltage regulator (AVR) was used for eliminating the oscillation of velocity in the test section of a subsonic wind tunnel due to the change of voltage.

5. Results and Discussion

5.1 Vector distribution of flow velocity

Figure 3 shows the vector distribution described by mean velocities U and V measured in the X-Y plane. This vector plot presents a symmetric distribution with respect to Y=0 as shown in Fig. 3, and the velocity ejected from about Y/R=±0.97 corresponding to the narrow slit is distributed with the largest magnitude. Consequently, some entrainment phenomena seem to appear in the outer region of Y/R=±0.97 because the stationary ambient air inflows and mixes into the main stream of a swirl burner. Here, because the rapid jet velocity ejected from the narrow slits and the flow velocity going out of swirl vanes etc. exist at the same time in this burner, the air stream ejected from the respective region of Y-direction up to about X/R=1.9 flows to downstream, and then mixes intensively with the rapid streamwise velocity. Consequently, the structure of two peaks exists in the forefront of the exit of a swirl burner, but the flow structure changes to four peaks as the flow develops to the streamwise direction. Therefore, above regions can be guessed as an initial region. However, the flow structure from a distance of X/R=2 develops with two peaks again smaller than those of an initial region. Moreover, the flow structure from a distance of X/R=7.8 has a constant non-dimensional velocity distribution because the flow seems to develop fully and the transverse slope of streamwise velocity completely seems to disappear.

Figure 4 shows the vector distribution described by mean velocities U and W measured in the X-Y plane. This vector plot also indicates a symmetric distribution in the whole flow fields with respect to Y=0 as shown in Fig. 4. The reason why this vector distribution presents a symmetric is because two swirl vanes situated in the left and right sides respectively in the inclined baffle plate as shown in Fig. 1 are not only located in the X-Y plane but also mutually symmetric with respect to the centerline, i. e., the flow going out of the left vane heads towards negative Z-direction with respect to the centerline, and the flow going out of the right vane vice versa. Consequently, the swirl vanes cause a counter-clockwise rotation flow when we see them on the front side of a swirl burner. Because the jet velocity ejected from about Y/R=±0.97 corresponding to the narrow slits is distributed with the largest magnitude as shown in Fig. 4, it plays a leading role for entrainment in the forefront of and in the outer region of the swirl burner. On the other hand, as the jet velocity ejected from the swirl vanes develops and diffuses toward the streamwise direction, the flow contraction phenomena can be seen up to the region of X/R=1.

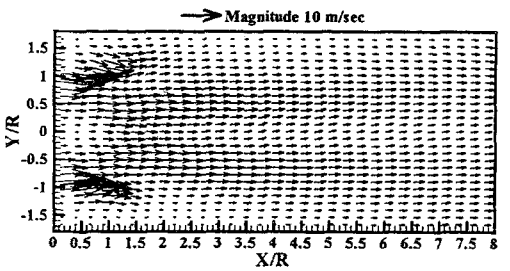

Fig. 3 Vector plot by mean velocities U and V measured in the X-Y plane

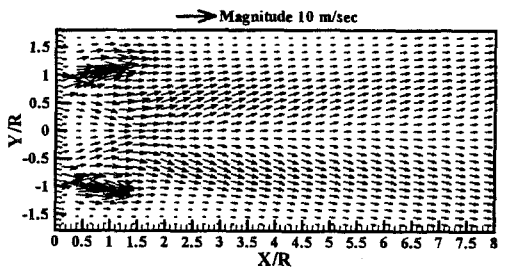

Fig. 4 Vector plot by mean velocities U and W measured in the X-Y plane

7 in the internal region of a swirl burner due to collision strength occurred by the flow velocity going out of the inclined vane with respect to the centerline. Therefore, the inclined angle of a cone type baffle plate has a great influence on the flow velocity formed within the range of X/R=1.7. But the flow velocity from a distance of X/R=1. 7 develops and diffuses toward the left and right sides of a swirl burner respectively.

5.2 Streamline distribution of flow velocity

Figure 5 indicates the streamline distribution obtained from the vector plot shown in Fig. 3. The flow diffusion and development process by means of the rapid jet velocity ejected from the narrow slits as shown in Fig. 5 can be more certainly seen through the streamline profile. The streamline formed in the outer region of the burner diffuses gradually and moves toward streamwise direction up to about X/R=3, but the streamline from a distance of X/R=3 gradually appears to be contracted somewhat toward the center region. Here, the entrainment, which the ambient air merges into the mainstream, seems to exist apparently in the initial outer region. Moreover, the streamlines corresponding to the rapid velocity mutually show a nearby neighboring distribution. On the other hand, the streamlines located in the inner region of the burner up to X/R=3 concentrate on the centerline by the comparatively more rapid streamwise flow velocity than the rotational flow going out of swirl vanes, but the streamlines after X/R=3 were apparently curved toward a swirling direction because the streamwise flow velocity decreases obviously and the rotational flow is highlighted.

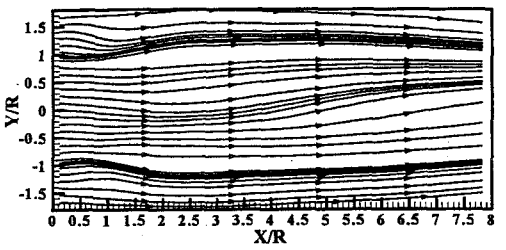

Fig. 5 Streamline plot by mean velocities U and V measured in the X-Y plane

Figure 6 indicates the streamline distribution obtained from the vector plot shown in Fig. 4. As the axial distance increases, the streamlines due to the rapid jet velocity ejected from the narrow slits as shown in Fig. 6 diffuse and develop continuously toward the left and right sides respectively with respect to the centerline. Especially, because the air stream going out of vanes situated on the inclined baffle plate jets to the centerline of the X-Y plane, the streamlines up to about X/R=1.7 are contracted, but the streamlines after a region of X/R=1.7 appear to be diffused toward the left and right side of a burner respectively. Consequently, the swirl effect of air stream apparently appears to counterclockwise rotation because the streamlines exist in large numbers toward the right side of a burner.

5.3 Mean velocity distribution

Figure 7 shows the non-dimensional mean velocity represented by dividing axial mean velocity U measured in the X-Y plane by upstream mean velocity U_0 of a swirl burner. Here, the mean velocity U is calculated by arithmetic mean between mean velocities U capable of obtaining respectively from the velocity pairs of (U, V) and (U, W) measured in the X-Y plane. The mean velocity U shown in Fig. 7 is largely formed until Y/R=±0.97 and X/R=1.5 due to the flow velocity ejected from the narrow slits because its contour is distributed very densely in this region. Moreover, the flow velocity going out of swirl vanes develops toward the inner region of the burner, and it diffuses and disappears as it goes downstream as shown in Fig. 7.

Figure 8 shows the non-dimensional mean velocity represented by dividing Y-directional

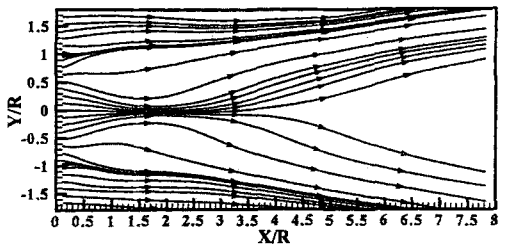

Fig. 6 Streamline plot by mean velocities U and W measured in the X-Y plane

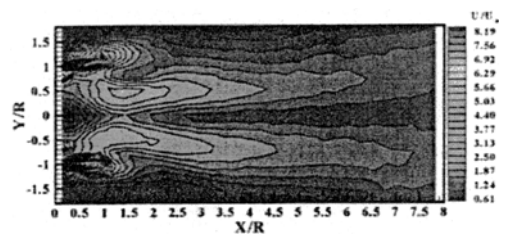

Fig. 7 Mean velocity U profile in the X-Y plane

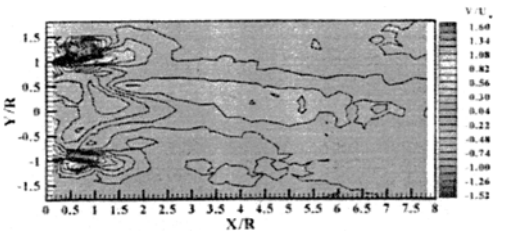

Fig. 8 Mean velocity V profile in the X-Y plane

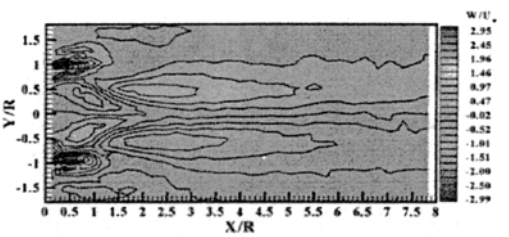

Fig. 9 Mean velocity W profile in the X-Y plane

component V of the mean velocity measured in the X-Y plane by upstream mean velocity U_0 of a swirl burner. The Y-directional mean velocity is largely formed at the narrow slits up to X/R=1.5, but the flow disappearing process can be seen after a region of X/R=1.5 because it has a comparatively small value. Particularly, the mean velocity V in the left side of a burner is distributed with the positive value because the flow moves from right side to centerline in terms of the inclined angle of flow going out of swirl vanes located on the left surface of a cone type baffle plate. However, in the case of the right side of a burner, the mean velocity V is distributed with the negative value because the flow moves from left side to centerline in terms of the inclined angle of flow.

Figure 9 shows the non-dimensional mean velocity represented by dividing Z-directional mean velocity W measured in the X-Y plane by upstream mean velocity U_0 of a swirl burner. The mean velocity W shows a comparatively symmetric distribution with respect to Y=0, and it is largely formed near the narrow slits located in the outer region of a burner up to X/R=1.5. However, the mean velocity W from a distance of X/R=1.5 is disappearing due to the diffusion from centerline to outer region even though its value is somewhat small. Moreover, the mean velocity W appears to the negative value in the left side of a burner because the Z-directional component of flow going out of a swirl vane located on the left surface of a cone type baffle plate heads downward, while in the case of the right side of a burner, it is distributed with the positive value because the Z-directional component of flow on the right part of a burner heads upward.

5.4 Turbulent intensity distribution

Figure 10 shows the X-directional component of turbulent intensity represented non-dimensionally by dividing RMS (Root-mean-square) u by upstream mean velocity U_0 of a swirl burner. The turbulent intensity u from Fig. 8 shows a comparatively symmetric distribution with respect to the centerline, and the value larger than about 71 % can be seen from inside and outside near the narrow slits corresponding to Y/R=±0.97 until X/R=1.5. Here, the reason why the turbulent intensity is distributed in large scale in the outer region of the burner is because the axial mean velocity of the flow ejected from the narrow slits is largely distributed in this region and the rotational flow due to the swirl vane also acts in it. Therefore, the transverse slope of axial mean velocity is formed very largely in this region. Kihm et al. (1990) early described that the swirler

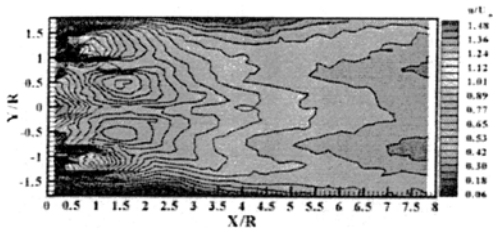

Fig. 10 Turbulent intensity u profile in the X-Y plane

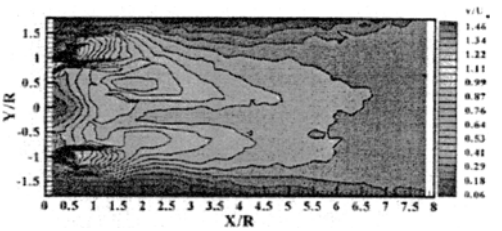

Fig. 11 Turbulent intensity v profile in the X-Y plane

brought about high turbulence intensities having a scale of above 100 %. Moreover, the turbulent intensity u in the central region increases up to about X/R=1.5. However, it decreases after X/R =1.5 as the axial distance increases. Consequently, the turbulent intensity u is distributed with a value comparatively larger than about 40 % over a wide range up to about X/R=6.3.

Figure 11 shows the Y-directional component of turbulent intensity represented non-dimensionally by dividing RMS v by upstream mean velocity U_0 of a swirl burner. The turbulent intensity v also shows a value larger than about 50 % from inside and outside near the narrow slits corresponding to Y/R=±0.97 until X/R=1.5. Moreover, the turbulent intensity v in the central region increases up to about X/R=1.5. However, it decreases from a distance of X/R=1.5 as the axial distance increases. Consequently, the turbulent intensity v with a value larger than about 40 % is distributed up to about X/R=3.8.

Figure 12 shows the Z-directional component of turbulent intensity represented non-dimensionally by dividing RMS w by upstream mean velocity U_0 of a swirl burner. The turbulent intensity w shows a comparatively symmetric distribution with respect to the centerline, and also the value larger than about 60 % can be seen from inside and outside near the narrow slits corresponding to Y/R=±0.97 until X/R=1.5. Moreover, the turbulent intensity w in the central region increases up to about X/R=1.5. However, it decreases after X/R=1.5 as the axial distance increases. Consequently, the turbulent intensity w is distributed with a value comparatively larger than about 40 % up to about X/R=4.

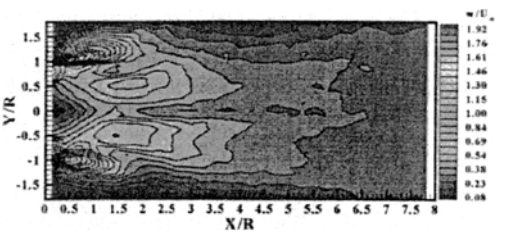

Fig. 12 Turbuilent intensity w profile in the X-Y plane

5.5 Turbulent kinetic energy distribution

Figure 13 shows the distribution of non-dimensional turbulent kinetic energy described by dividing the turbulent kinetic energy obtained from Eq. (4) by upstream mean velocity U_0^2 of a swirl burner.

Here, the turbulent kinetic energy is defined as follows:

$$KE=\frac{1}{2}(u^2+v^2+w^2) \tag{4}$$

where u^2, v^2 and w^2 are Reynolds normal stresses or variances of turbulence.

The turbulent kinetic energy like a turbulent intensity shows a symmetric distribution with respect to the centerline, and the value larger than about 73 % appears from inside and outside near the narrow slits corresponding to Y/R=±0.97 up to X/R=1.5. Moreover, the turbulent kinetic energy in the central region increases up to about X/R=1.5. However it decreases from a distance of X/R=1.5 as the axial distance increases. Consequently, the turbulent kinetic energy is distributed with a value comparatively larger than about 34 % up to about X/R=3 corresponding to the relatively initial region.

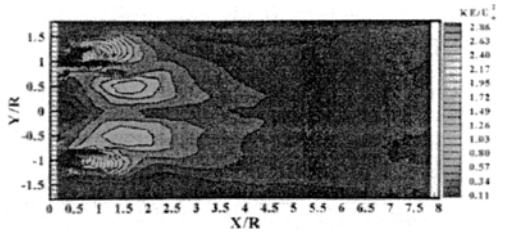

Fig. 13 Turbulent kinetic energy profile in the X-Y plane

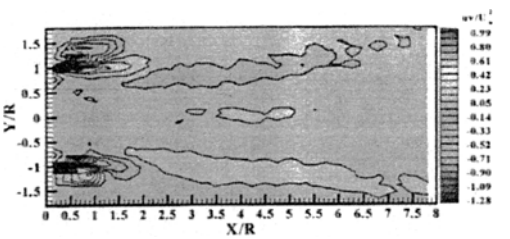

Fig. 14 Reynolds shear stress uv profile in the X-Y plane

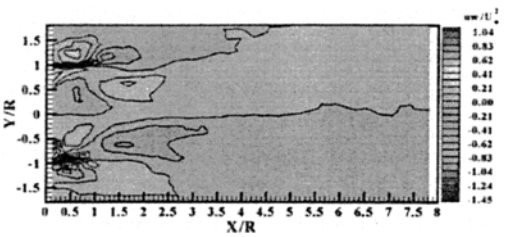

Fig. 15 Reynolds shear stress uw profile in the X-Y plane

5.6 Reynolds shear stress distribution

Figure 14 shows the non-dimensional turbulent shear stress represented by dividing Reynolds shear stress uv measured in the X-Y plane by upstream mean velocity U_0^2 of a swirl burner. Reynolds shear stress uv shows a large value near the narrow slits. Especially, the positive and negative peak values exist in the left inside and right outside of $Y/R=0.97$ respectively, while the positive and negative peak values exist in the left outside and right inside of $Y/R=-0.97$ respectively. This is due to the transverse slope of a mean velocity with respect to the respective direction. Consequently, the negative value is mainly distributed in the left side of internal region of the burner, but the positive value is distributed in the right side up to near $X/R=2$. However, after a region of $X/R=2$, the negative value is formed in the right side of a burner as shown in Fig. 14, and the positive value vice versa. Kihm et al. (1990) described that the Reynolds shear stress has both negative and positive values associated with the positive and negative gradients of the mean velocity profiles. For swirling flows, the turbulent shear stress distribution is strongly non-isotropic, and it is a function of the degree of swirl and position in the flow field. (Lilley et al., 1971)

Figure 15 shows the non-dimensional turbulent shear stress represented by dividing Reynolds shear stress uw measured in the X-Y plane by upstream mean velocity U_0^2 of a swirl burner. Reynolds shear stress uw shows a relatively large value smaller than uv near the narrow slits. Moreover, the positive and negative peak values exist in the right outside and left inside of $Y/R=0.97$ respectively up to $X/R=1$, while the positive and negative peak values exist in the right inside and left outside of $Y/R=-0.97$ respectively. However, after a region of $X/R=1$, the peak value of uw is distributed with a different sign of the exact opposite to that of uv. Moreover, the right side with respect to Y-axis shows a positive value in the above region of $X/R=2.5$, and the left side vice versa.

6. Conclusion

In view of the results so far achieved through the turbulent flow fields measured in the X-Y plane of the gas swirl burner with a cone type baffle plate by using an X-type hot-wire, the axial mean velocity, the turbulent intensities, the turbulent kinetic energy and the Reynolds shear stresses of the flow ejected from the narrow slits corresponding to $Y/R=\pm0.97$ are distributed respectively with the largest magnitude up to $X/R=1.5$. Moreover, they show a relatively large value in the inner region of the burner due to the flow diffusion and mixing processes between the inclined baffle plate and the swirl vane. Consequently the combustion reaction is expected to occur actively near this region. Especially, the inclined angle of a cone type baffle plate seems to affect up to $X/R=1.5$. The rotational flow can be

shown in the inner region of the burner because the mean velocity W is distributed with the magnitude larger than V due to the inclined flow velocity ejecting from the swirl vanes. Moreover, the Reynolds shear stresses uv and uw are largely distributed respectively near the narrow slits of a burner.

Acknowledgement

This paper is partially supported by the Fisheries Science Institute of Kunsan National University in 2000.

References

Aoki K., Nakayama Y. and Wakatsuki M., 1988, "Study on the Cylindrical Combustor Flow with Swirling Flow (1st Report, Characteristics of Flow Pattern for Swirling Number)," *Transactions of JSME (Part B)*, Vol. 51, No. 468, pp. 2759~2766 (In Japanese).

Aoki K., Shibata M. and Nakayama Y., 1989, "Study on the Cylindrical Combustor Flow with Swirling Flow (2nd Report, Characteristics of Turbulence for Swirling Number)," *Transactions of JSME (Part B)*, Vol. 52, No. 476, pp. 1617~1625 (In Japanese).

Beer J. M. and Chigier N. A., 1972, *Combustion Aerodynamics*, Applied Science Publishers, pp. 100~146.

Bruun H. H., 1996, *Hot-Wire Anemometry*, Oxford Science Publications, pp. 132~163.

Dantec, 2000, *Streamline User's Reference Manual*, Chapter 8.3 Algorithms.

Hirai, T., Nagai, N., Koseki, H., Kato, K., and Takado, J., 1988, "Study on Spray Combustion Characteristics of a High Intensity Swirl Combustor (1st Report, Combustion Characteristics of Kerosene Spray)," *Transactions of JSME (Part B)*, Vol. 51, No. 463, pp. 1077~1082 (In Japanese).

Ikeda Y., Kawahara N. and Nakayima T., 1995, "Flux Measurements of O_2, CO_2 and NO in Oil Furnace," *Transactions of JSME (Part B)*, Vol. 61, No. 581, pp. 332~338 (In Japanese).

Kihm, K. D., Chigier, N., and Sun, F., 1990, "Laser Doppler Velocimetry Investigation of Swirler Flowfields," *J. Propulsion*, Vol. 6, No. 4, pp. 364 ~374.

Kim, I. K., 1997, "The Study on Flame Structure and Characteristics of Gun Type Burner for Different Type of Flame Holder," Master Thesis, Pusan National University, pp. 43~46 (In Korean).

Kim, I. K., Youn, W. H., Ha, M. Y. and Kim, Y. H., 1998, "The Study on Flow and Combustion Characteristics of Gun-Type Gas Burner," *Proceedings of the KSME Spring Annual Meeting B*, pp. 284~289 (In Korean).

Kim, J. K., Jeong, K. J., Kim, S. W. and Kim, I. K., 2000, "Investigation of the Three-dimensional Turbulent Flow Fields in Cone Type Gas Burner for Furnace," *Journal of KSPSE*, Vol. 4, No. 4, pp. 25~31 (In Korean).

Kim, J. K., 2001, "An Experimental Study on the Three Dimensional Turbulent Flow Characteristics of Swirl Burner for Gas Furnace," *Transactions of KSME (Part B)*, Vol. 25, No. 2, pp. 225~234 (In Korean).

Kurihara N., Ikeda Y. and Nakajima T., 1994, "Spray Behavior and Its Interaction with Turbulent Air Flow on Gun-Type Burner," *Transactions of JSME (Part B)*, Vol. 60, No. 570, pp. 656~661 (In Japanese).

Kurihara N., Ikeda Y. and Nakajima T., 1995, "Dispersion Process of the Formed by an Air-Assisted Injector," *Transactions of JSME (Part B)*, Vol. 61, No. 582, pp. 759~764 (In Japanese).

Lilley, D. G. and Chigier, N. A., 1971, "Nonisotropic Turbulent Shear Stress Distribution in Swirling Flows from Mean Value Distributions," *International Journal of Heat and Mass Transfer*, Vol. 14, pp. 573~585.

Yoon, W. H., 1999, "The Numerical Study on the Flow and Combustion Characteristics of Gas Swirl Burner," Master Thesis, Pusan National University, pp. 7~39 (In Korean).